Senescence-associated SIN3B promotes inflammation and pancreatic cancer progression

Maïté Rielland,[1] David J. Cantor,[1] Richard Graveline,[1] Cristina Hajdu,[2] Lisa Mara,[2] Beatriz de Diego Diaz,[1] George Miller,[3,4] and Gregory David[1,5]

[1]Department of Biochemistry and Molecular Pharmacology, [2]Department of Pathology, [3]Department of Surgery, [4]Department of Cell Biology, and [5]New York University (NYU) Cancer Institute, NYU School of Medicine, New York, New York, USA.

Pancreatic ductal adenocarcinoma (PDAC) is strikingly resistant to conventional therapeutic approaches. We previously demonstrated that the histone deacetylase–associated protein SIN3B is essential for oncogene-induced senescence in cultured cells. Here, using a mouse model of pancreatic cancer, we have demonstrated that SIN3B is required for activated KRAS-induced senescence in vivo. Surprisingly, impaired senescence as the result of genetic inactivation of *Sin3B* was associated with delayed PDAC progression and correlated with an impaired inflammatory response. In murine and human pancreatic cells and tissues, levels of SIN3B correlated with KRAS-induced production of IL-1α. Furthermore, evaluation of human pancreatic tissue and cancer cells revealed that Sin3B was decreased in control and PDAC samples, compared with samples from patients with pancreatic inflammation. These results indicate that senescence-associated inflammation positively correlates with PDAC progression and suggest that SIN3B has potential as a therapeutic target for inhibiting inflammation-driven tumorigenesis.

Introduction

Pancreatic ductal adenocarcinoma (PDAC) is a deadly disease, with a median survival of approximately 6 months. Although surgery offers the potential for long-term survival, the typical presentation of advanced disease at diagnosis often precludes surgery as an option (1). Thus, it is important to understand the molecular bases for progression of the disease in order to devise improved approaches for early intervention. Molecular pathology studies of human specimens and the development of genetically engineered mouse models have demonstrated that PDAC arises from noninvasive precursor lesions known as pancreatic intraepithelial neoplasia (PanIN), which are driven by activating *KRas* mutations (1–5). While endogenous expression of oncogenic *KRas* (*KRas*^{G12D}) leads to PanIN lesions in the mouse, the progression to PDAC requires additional mutations in genes such as *p53* or *Ink4a/Arf*. These mutations promote cellular proliferation in the presence of an activated oncogene in vitro and are detected in high-grade PanIN lesions and PDAC in human specimens (2, 4, 6–8).

Cellular senescence is an irreversible cell-cycle arrest triggered by different stimuli, including oxidative stress, DNA damage, and oncogene activation, that prevents damaged or mutated cells from proliferating uncontrollably (9). Senescence is associated with low proliferation in a wide variety of cancer preneoplastic lesions, including lung adenoma, melanocytic naevi, and PanIN (8, 10–12). Through its ability to drive a potent cell-cycle exit, cellular senescence has long been considered a tumor-suppressive mechanism (9, 13, 14). Recently, it was demonstrated that senescent cells secrete a specific set of proinflammatory cytokines, including ILs (such as IL-1α, IL-1β, IL-6, and IL-8), chemokines, and growth factors, known collectively as the senescence-associated secretory phenotype (SASP) (15–17). In contrast with the tumor-suppressing impact of senescence-associated cell-cycle arrest, in vitro studies suggest that the SASP may promote a protumorigenic microenvironment (18–21). This notion is particularly relevant to PDAC, as its progression is intimately linked to inflammation (1, 22–26). The cellular factors that contribute to the oncogene-driven inflammation in pancreatic cells remain for the most part unknown, but recent studies have implicated IL-1α expression as an inducer of constitutive NF-κB activation and subsequent inflammation (27–30). Identifying unsuspected druggable targets driving KRAS-induced inflammatory response could lead to the development of novel therapeutic approaches for targeting the disease at stages where treatment may be most effective.

SIN3 proteins are noncatalytic scaffolding proteins that serve as evolutionarily conserved components of the histone deacetylase HDAC1/2 transcriptional repression complex (31, 32). We have recently demonstrated that mouse embryonic fibroblasts genetically inactivated for *Sin3B* are refractory to quiescence as well as oncogene-induced senescence (33–35). In addition, SIN3B levels are significantly upregulated in preneoplastic senescent lesions in a mouse model of PDAC (34). Unlike most perturbations that bypass oncogene-induced senescence, *Sin3B* inactivation is not sufficient to sensitize to oncogenic RAS-induced transformation, providing an experimental context in which these processes are uncoupled (34). Therefore, genetic inactivation of *Sin3B* represents a unique opportunity to dissect the physiological relevance of cellular senescence in pancreatic cancer progression. Using this approach, we demonstrate here that the inactivation of *Sin3B* in the pancreas prevents oncogenic KRAS-induced senescence, correlating with a defect in the proinflammatory phenotype, ultimately resulting in delayed pancreatic cancer progression.

Results

Genetic inactivation of Sin3B delays progression of KRAS^{G12D}*-driven pancreatic lesions*. To examine the potential significance of SIN3B upregulation in PanIN lesions (34), mice carrying a *Sin3B* condi-

Conflict of interest: The authors have declared that no conflict of interest exists.
Citation for this article: *J Clin Invest.* 2014;124(5):2125–2135. doi:10.1172/JCI72619.

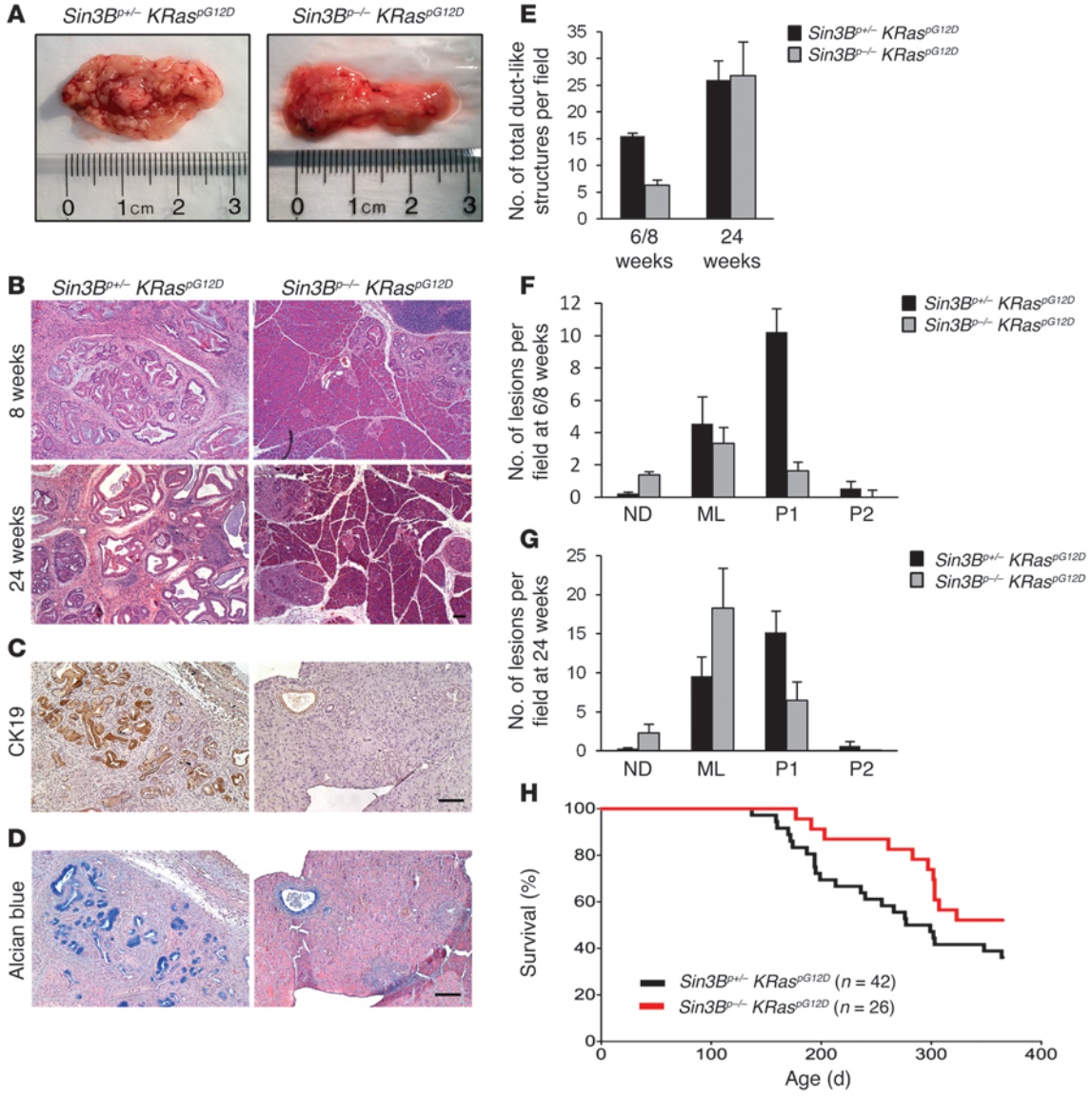

Figure 1

Genetic inactivation of *Sin3B* delays progression of KRAS^{G12D}-driven PanINs. (**A**) Representative 6-month-old pancreata from *Sin3B*$^{p+/-}$ *Kras*^{pG12D} and *Sin3B*$^{p-/-}$ *Kras*^{pG12D} mice. (**B**) H&E staining in 8- and 24-week-old *Sin3B*$^{+/}$ *Kras*^{pG12D} and *Sin3B*$^{p-/-}$ *Kras*^{pG12D} pancreata. (**C**) Immunochemistry for CK19 in 8-week-old *Sin3B*$^{+/-}$ *Kras*^{pG12D} and *Sin3B*$^{p-/-}$ *Kras*^{pG12D} pancreata. (**D**) Alcian blue staining for mucin in 8-week-old *Sin3B*$^{+/-}$ *Kras*^{pG12D} and *Sin3B*$^{p-/-}$ *Kras*^{pG12D} pancreata. (**E**) Number of duct-like structures per field in 6- to 8-week-old (6/8 weeks) and 24-week-old pancreata. Black bars represent *Sin3B*$^{p+/-}$ *Kras*^{pG12D} pancreas and gray bars represent *Sin3B*$^{p-/-}$ *Kras*^{pG12D} pancreas. (**F**) Number of normal ducts (ND), metaplastic lesions (ML), PanIN1 (P1), PanIN2 (P2), and PanIN3 (P3) per field in 6- to 8-week-old mice. Black bars represent *Sin3B*$^{p+/-}$ *Kras*^{pG12D} pancreas, and gray bars represent *Sin3B*$^{p-/-}$ *Kras*^{pG12D} pancreas. (**G**) Number of normal ducts, metaplastic lesions, PanIN1, PanIN2, and PanIN3 per field in 24-week-old mice. Black bars represent *Sin3B*$^{p+/-}$ *Kras*^{pG12D} pancreas, and gray bars represent *Sin3B*$^{p-/-}$ *Kras*^{pG12D} pancreas. (**H**) Kaplan-Meier Survival curve of *Sin3B*$^{p+/-}$ *Kras*^{pG12D} mice (black, $n = 42$) and *Sin3B*$^{p-/-}$ *Kras*^{pG12D} mice (red, $n = 26$). $P < 0.05$ at 300 days.

tional allele were first crossed with transgenic mice expressing the *Cre* recombinase under the control of the pancreas-specific *p48* promoter (35, 36). *Sin3B*$^{flox/+}$ *p48-Cre*$^{+}$ and *Sin3B*$^{flox/-}$ *p48-Cre*$^{+}$ animals (hereafter referred to as *Sin3B*$^{p+/-}$ and *Sin3B*$^{p-/-}$) were born at the expected ratio (data not shown). *Sin3B*$^{p+/-}$ animals were used as controls, as heterozygote animals are phenotypically indistinguishable from *Sin3B*$^{+/+}$ animals through 16 months of age (data not shown and ref. 35). Similar to the control littermates, *Sin3B*$^{p-/-}$ animals exhibited no gross abnormalities up to 1 year of age and presented normal pancreatic morphology (Supplemental Figure 1A and data not shown; supplemental material available online with this article; doi:10.1172/JCI72619DS1). Transcript analysis and immunohistochemistry (IHC) confirmed the efficient *Sin3B* inactivation in *Sin3B*$^{p-/-}$ pancreata (Supplemental Figure 1, A and B). Of note, the residual *Sin3B* expression detected in *Sin3B*$^{p-/-}$ pancreata likely reflects the heterogeneity of the pancreas tissue, which contains circulating blood cells that are not affected by *p48-Cre*–induced deletion (Supplemental Figure 1B). Finally, the exocrine and endo-

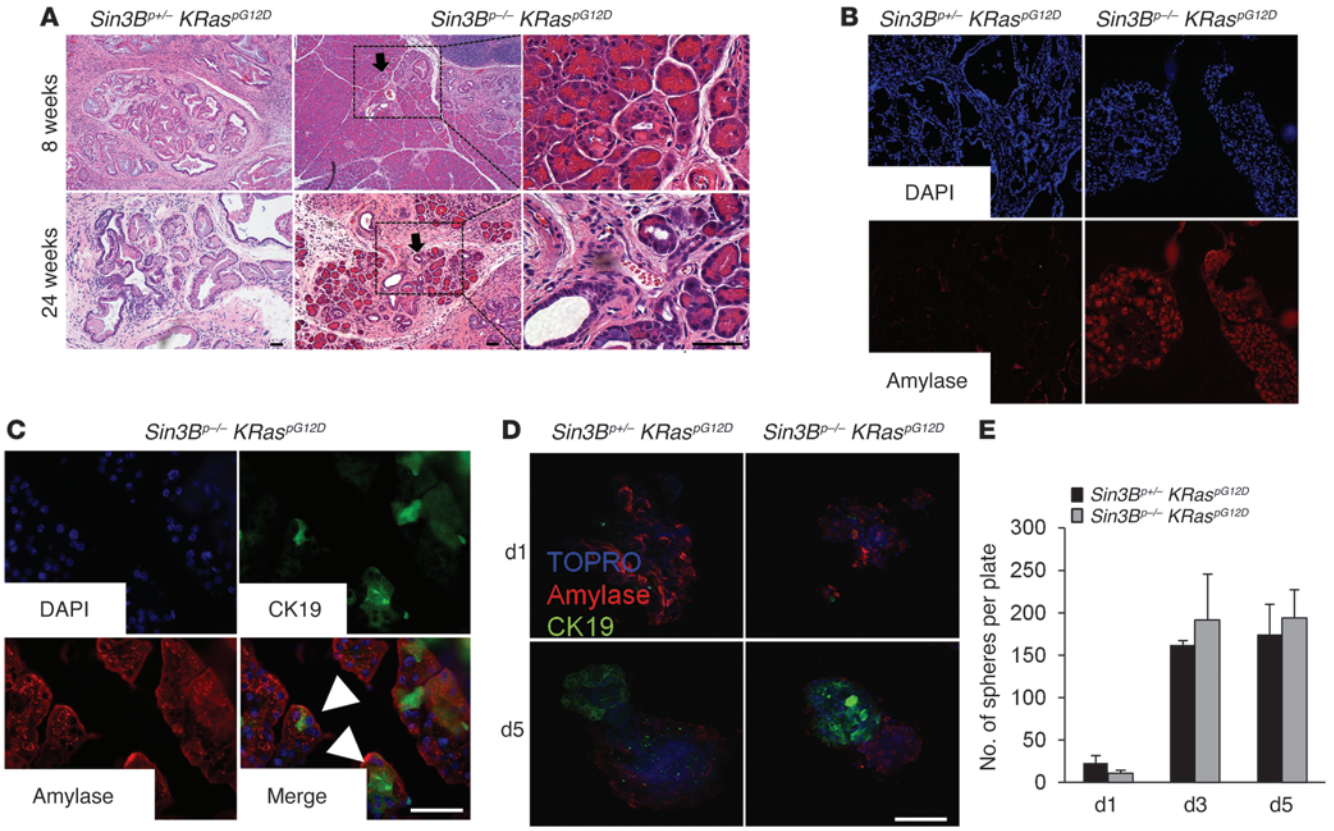

Figure 2

Sin3B deletion does not affect the ADM process in a cell-autonomous manner. (**A**) H&E staining of paraffin sections of pancreas obtained from 8- and 24-week-old *Sin3B*$^{p+/-}$ *Kras*^{pG12D} and *Sin3B*$^{p-/-}$ *Kras*^{pG12D} mice. (**B**) Immunofluorescence on cryogenic sections of 6-week-old *Sin3B*$^{p+/-}$ *Kras*^{pG12D} and *Sin3B*$^{p-/-}$ *Kras*^{pG12D} pancreata using anti–α-amylase antibody (red). Nuclei are counterstained with DAPI in blue. (**C**) Immunofluorescence on cryogenic sections of *Sin3B*$^{p-/-}$ *Kras*^{pG12D} pancreas using anti–α-amylase antibody (red) and anti-CK19 antibody (green). Nuclei are counterstained with DAPI (blue). (**D**) Immunofluorescence on the 3D structure obtained from acinar cells isolated from *Sin3B*$^{p+/-}$ *Kras*^{pG12D} and *Sin3B*$^{p-/-}$ *Kras*^{pG12D} pancreata 1 day (d) and 5 days after plating in 3D culture using anti–α-amylase antibody (red) and anti-CK19 antibody (green). Nuclei are counterstained with toproisomerase (TOPRO, blue). (**E**) Number of sphere-like structures obtained from acinar cells isolated from *Sin3B*$^{p+/-}$ *Kras*^{pG12D} (black bars, $n = 3$) and *Sin3B*$^{p-/-}$ *Kras*^{pG12D} (gray bars, $n = 3$) pancreata at 1 day, 3 days, and 5 days after plating in 3D culture. Scale bars: 50 μm (**A**, **B**); 25 μm (**C**, **D**).

crine functions of the pancreas appeared largely unaffected by the genetic inactivation of *Sin3B*, as evidenced by the production of amylase and insulin in both *Sin3B*$^{p+/-}$ and *Sin3B*$^{p-/-}$ pancreata (Supplemental Figure 1, C and D). Thus, SIN3B appears largely dispensable for the development and normal function of the pancreas.

We next investigated whether *Sin3B* inactivation affects the progression of *KRas*^{G12D}-driven PanINs by crossing *Sin3B*$^{p-/-}$ mice with *Cre*-inducible Lox-STOP-Lox-*KRas*^{G12D} mice (37). All genotypes (including *Sin3B*$^{p+/-}$ *KRas*^{pG12D} and *Sin3B*$^{p-/-}$ *KRas*^{pG12D}) were detected at the expected ratio (data not shown), and efficient *Sin3B* deletion was confirmed (Supplemental Figure 1, E and F). While the pancreata of 24-week-old *Sin3B*$^{p+/-}$ *KRas*^{pG12D} mice was granular with abundant pale nodules throughout, signaling the presence of numerous metaplastic and PanIN lesions, the pancreata of their *Sin3B*-deleted littermates (*Sin3B*$^{p-/-}$ *KRas*^{pG12D}) exhibited normal gross appearance (Figure 1A). Histologic examination of additional animals at different time points revealed PanIN surrounded by extensive fibrosis as early as 6 to 8 weeks and progressively higher grade lesions in *Sin3B*$^{p+/-}$ *KRas*^{pG12D} mice (Figure 1B), as previously reported (2). In stark contrast, pancreata from *Sin3B*$^{p-/-}$ *KRas*^{pG12D} mice comprised of mostly normal acini with rare metaplastic areas and early PanINs, up to 24 weeks of age (Figure 1B) ($n > 10$ mice for each genotype). These morphologic findings were corroborated by staining for CK19 and Alcian blue, which together mark mucin-containing PanIN cells (Figure 1, C and D). Quantification of CK19-positive structures indicated significantly fewer duct-like structures at 6 to 8 weeks (Figure 1, E and F) and a delay in the progression of the pancreatic lesions at 24 weeks (Figure 1, E and G) in *Sin3B*$^{p-/-}$ *KRas*^{pG12D} mice compared with their *Sin3B*$^{p+/-}$ *KRas*^{pG12D} littermates. Furthermore, the pancreata of *Sin3B*$^{p-/-}$ *KRas*^{pG12D} animals older than 6 months of age also displayed a significantly higher percentage of normal acini compared with *Sin3B*$^{p+/-}$ *KRas*^{pG12D} animals ($P < 0.001$) (Supplemental Table 2). Finally, mortality was also significantly delayed upon *Sin3B* deletion in *KRas*-expressing mice (Figure 1H, $P < 0.05$ at 300 days, and Supplemental Table 1). Of note, *Sin3B*$^{p-/-}$ *KRas*^{pG12D} mice finally developed PDAC later in life, as indicated by the drop in viability in these mice past 1 year (Supplemental Tables 1–3). Strikingly, most of the tumor cells in the *Sin3B*$^{p-/-}$ *KRas*^{pG12D} PDAC expressed SIN3B (Supplemental Figure 1G). Along with the near complete deletion of SIN3B observed

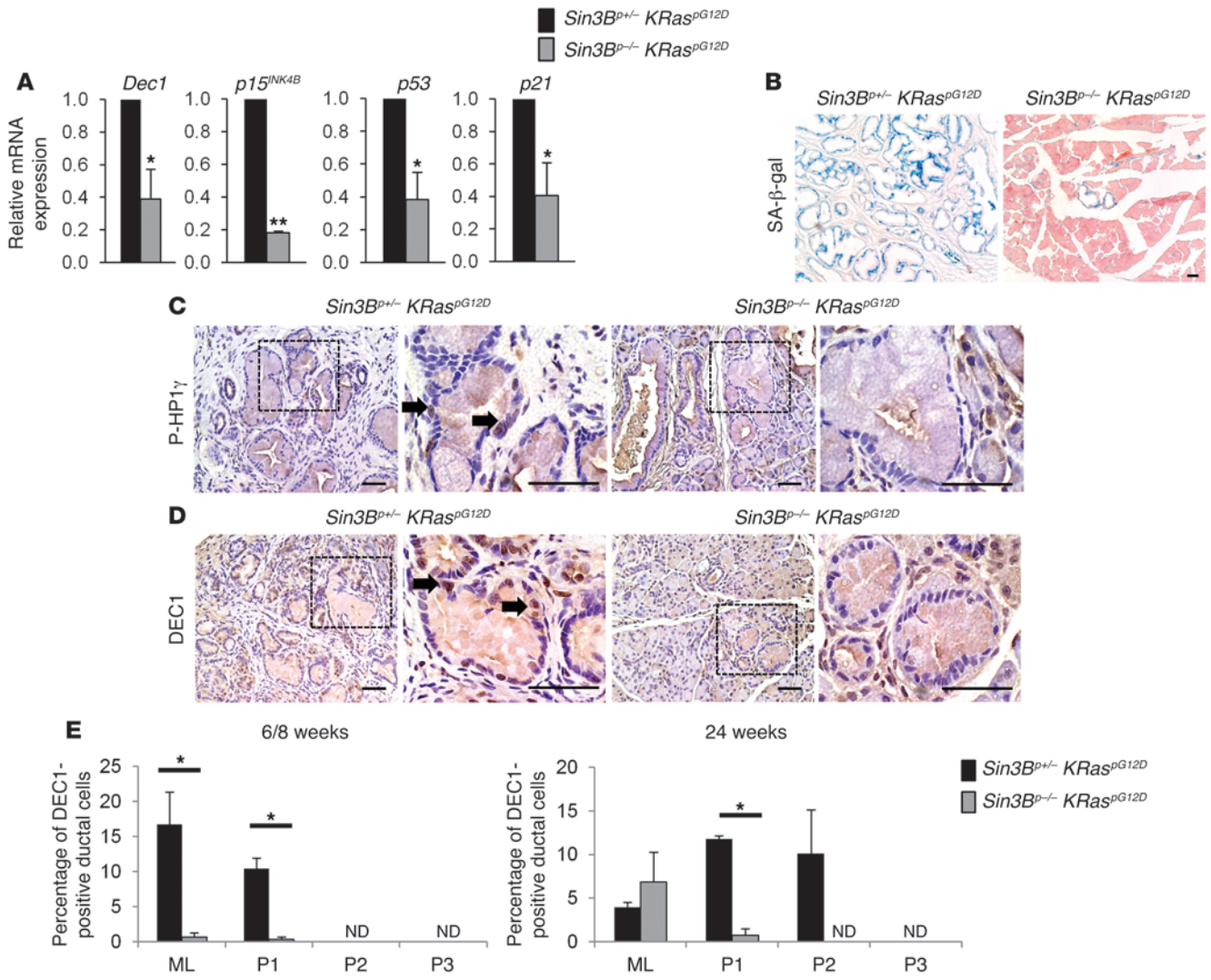

Figure 3

Sin3B deletion impairs oncogene KRAS-induced senescence in vivo. (**A**) Quantitative PCR for *Dec1*, *p15*^{INK4B}, *p53*, and *p21* mRNA expression in pancreata obtained from 6- to 8-week-old *Sin3B*$^{p+/-}$ *Kras*^{pG12D} (black bars, $n = 3$) and *Sin3B*$^{p-/-}$ *Kras*^{pG12D} (gray bars, $n = 3$) mice. *Sin3B*$^{p-/-}$ *Kras*^{pG12D} expression is relative to *Sin3B*$^{p+/-}$ *Kras*^{pG12D} expression. *$P < 0.05$; **$P < 0.00001$. (**B**) Cryogenic sections stained for SA–β-gal in *Sin3B*$^{p+/-}$ *Kras*^{pG12D} and *Sin3B*$^{p-/-}$ *Kras*^{pG12D} pancreata. (**C**) Immunochemistry for p-HP1γ on paraffin sections of 8-week-old *Sin3B*$^{p+/-}$ *Kras*^{pG12D} and *Sin3B*$^{p-/-}$ *Kras*^{pG12D} pancreata. (**D**) Immunochemistry for DEC1 on paraffin sections of 8-week-old *Sin3B*$^{p+/-}$ *Kras*^{pG12D} and *Sin3B*$^{p-/-}$ *Kras*^{pG12D} pancreata. Arrows indicate positively stained cells. Scale bars: 50 μm. (**E**) Percentage of DEC1-positive ductal cells at 6 to 8 weeks and at 24 weeks in *Sin3B*$^{p+/-}$ *Kras*^{pG12D} and *Sin3B*$^{p-/-}$ *Kras*^{pG12D} pancreata. ND, not detected. *$P < 0.05$.

in younger mice (Supplemental Figure 1, E and F), this observation suggests that *Sin3B* inactivation is potently counterselected to allow PDAC progression. Thus, these results strongly support the notion that SIN3B promotes KRAS-driven cancer progression upon KRAS activation.

Sin3B deletion does not affect the ADM process in a cell-autonomous manner. Recent lineage-tracing studies indicate that the majority of human and mouse PanIN lesions result from the transdifferentiation of acinar cells into ductal cells through a process known as acinar-to-ductal metaplasia (ADM) (38–40). Based on our finding that KRAS-expressing, *Sin3B*-deleted pancreata contained significantly more acini and fewer PanINs compared with their *Sin3B*-expressing littermates, we investigated whether the ADM process was impaired. Histologic observations (Figure 2A) and the overall reduction of amylase staining (Figure 2B) strongly suggested that ADM had already occurred and was completed by 8 weeks of age in *Sin3B*$^{p+/-}$*Kras*^{pG12D} pancreata. In contrast, ADM was still observed in 8-week-old *Sin3B*$^{p-/-}$ *Kras*^{pG12D} animals, as evidenced by frequent coexpression of amylase and CK19, suggesting that SIN3B delays the initiation or impairs the maintenance of ADM lesions in vivo (Figure 2C). To assess whether SIN3B regulates ADM in a cell-autonomous manner, acinar cells from 5 week-old *Sin3B*$^{p+/-}$ *Kras*^{pG12D} mice and their *Sin3B*$^{p-/-}$ *Kras*^{pG12D} littermates (Supplemental Figure 2A) were cultured using a 3D matrix (41). Amylase expression was detectable in acini of both genotypes upon initial isolation, and these cells progressively underwent ADM, as evidenced by an increase in CK19 staining and formation of sphere-like structures by day 5 (Figure 2D). The efficiency of sphere formation was not

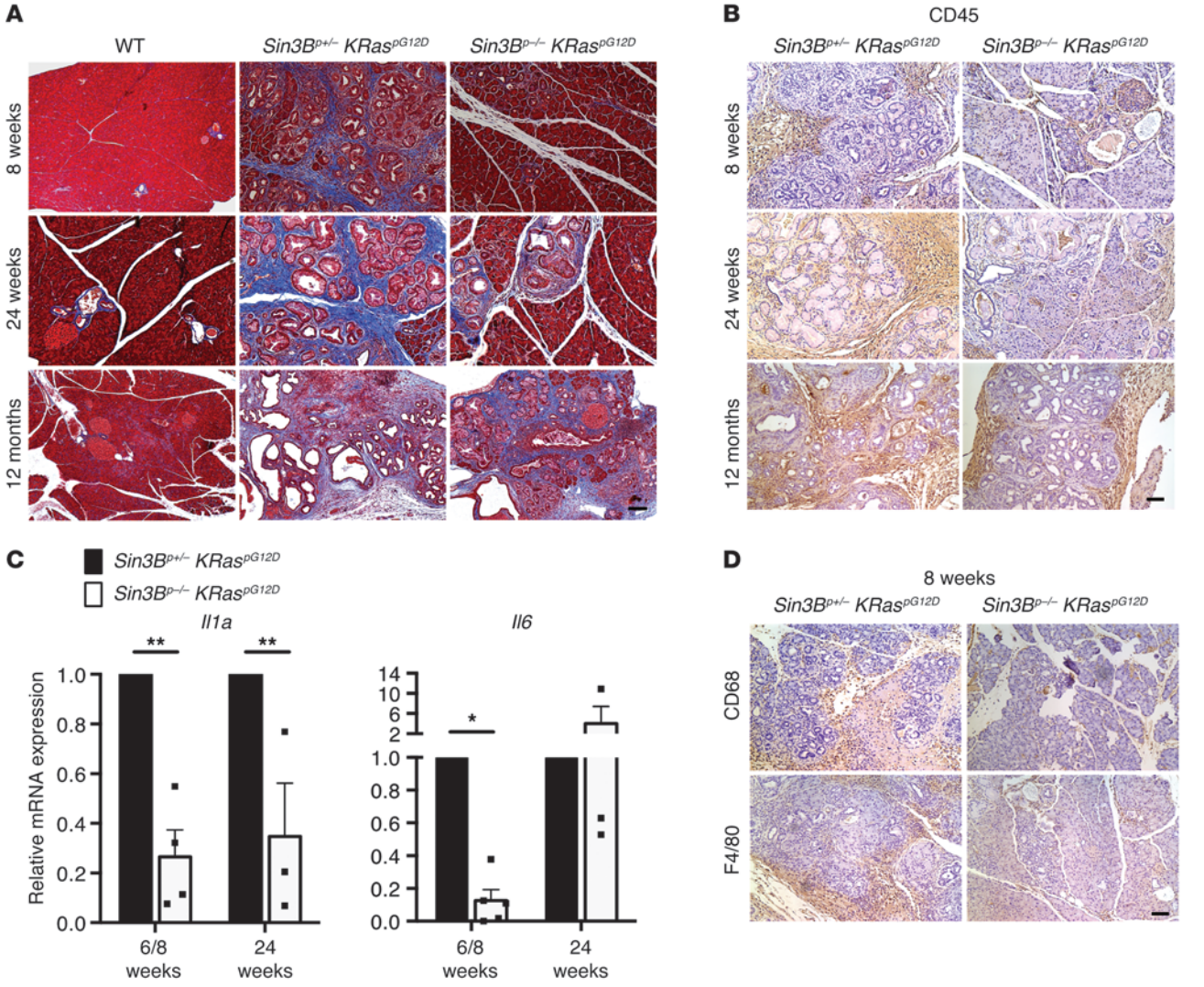

Figure 4

Loss of SIN3B mitigates oncogenic KRAS-driven inflammatory response in vivo. (**A**) Masson trichrome staining of paraffin sections of 8-week-old, 24-week-old, and 12-month-old WT, *Sin3B*$^{p+/-}$ *Kras*^{pG12D}, and *Sin3B*$^{p-/-}$ *Kras*^{pG12D} mice. (**B**) IHC for CD45 in pancreata obtained from 8-week-old, 24-week-old, and 12-month-old *Sin3B*$^{p+/-}$ *Kras*^{pG12D} and *Sin3B*$^{p-/-}$ *Kras*^{pG12D} mice. (**C**) Quantitative PCR for *Il6* and *Il1a* mRNA expression in pancreata obtained from 6- and 8-week-old (6/8 weeks) and 24-week-old *Sin3B*$^{p+/-}$ *Kras*^{pG12D} and *Sin3B*$^{p-/-}$ *Kras*^{pG12D} mice. Black bars represent *Sin3B*$^{p+/-}$ *Kras*^{pG12D} pancreas, and gray bars represent *Sin3B*$^{p-/-}$ *Kras*^{pG12D} pancreas. *Sin3B*$^{p-/-}$ *Kras*^{pG12D} mRNA expression levels are relative to the *Sin3B*$^{p+/-}$ *Kras*^{pG12D} expression levels. *$P < 0.01$; **$P < 0.05$. (**D**) IHC for CD68 and F4/80 in pancreata obtained from 8-week-old *Sin3B*$^{p+/-}$ *Kras*^{pG12D} and *Sin3B*$^{p-/-}$ *Kras*^{pG12D} mice. Scale bars: 50 μm.

significantly affected by *Sin3B* deletion (Figure 2E and Supplemental Figure 2B). Together, these results indicate that ADM initiation and efficiency are not affected by *Sin3B* inactivation in vitro. However, because we found that the ADM process is delayed in vivo, we hypothesized that SIN3B could promote pancreatic cancer progression in a non–cell autonomous manner.

Sin3B deletion impairs oncogene KRAS-induced senescence in vivo. Recent work has established that senescent cells alter their microenvironment by secreting inflammatory factors, growth factors, and remodeling factors in a process called SASP. SASP triggers senescence in neighboring cells and mobilizes immune cells, but can also induce inflammation and thus promote cancer progression (18, 42, 43). This phenomenon is particularly relevant in pancreatic cancer, where inflammation is a well-established factor in tumor progression (23, 26). Based on our recent discovery that SIN3B is required for oncogene-induced senescence in mouse embryonic fibroblasts (34), we investigated whether *Sin3B* deletion affects the senescence process in pancreatic lesions. Consistent with a direct role of SIN3B in oncogenic KRAS-induced senescence in vivo, *Sin3B*$^{p-/-}$ *KRas*^{pG12D} pancreata displayed significantly reduced expression levels of senescence markers, including *Dec1*, *p15INK4B*, *p21*, and *p53* as compared with those observed in *Sin3B*$^{p+/-}$ *KRas*^{pG12D} littermates (Figure 3A). Accordingly, senescence-associated β-gal (SA–β-gal) positivity (44) was markedly reduced in *Sin3B*-deficient pancreata (Figure 3B). Recent studies suggested that SA–β-gal positivity alone cannot be used to definitely specify senescent cells in the pancreas (11). We further probed, by IHC analysis, the presence of phosphorylated HP1γ (p-HP1γ) and DEC1,

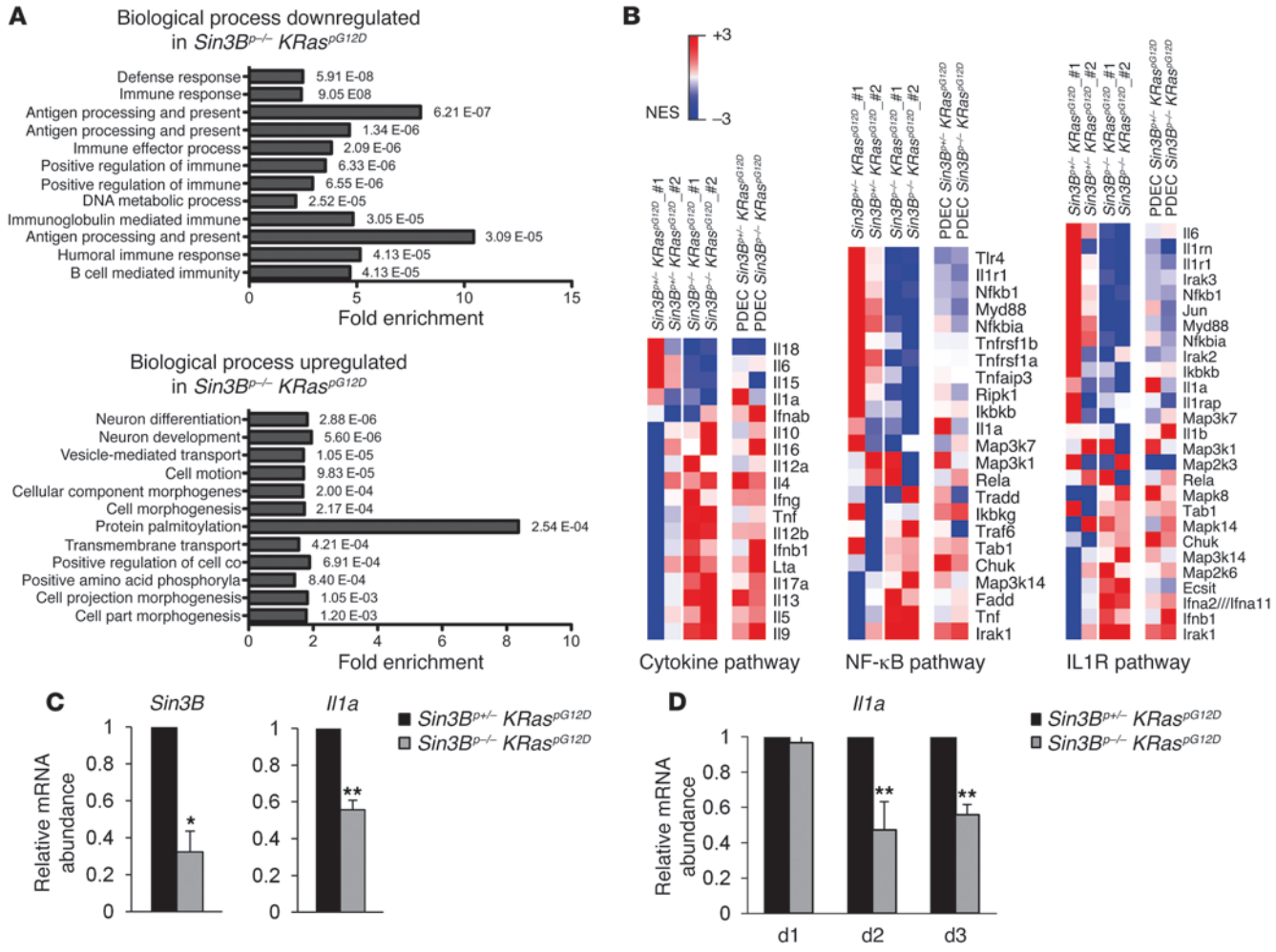

Figure 5

SIN3B is required for cell-autonomous *Il1a* expression. (**A**) Pathway enrichment analysis using DAVID gene ontology for genes affected transcriptionally by *Sin3B* deletion. Pathway enrichment shows genes transcriptionally repressed (top) or induced (bottom) after *Sin3B* deletion in *Kras^{pG12D}* pancreas. GO analyses were made on genes that presented at least a 1.5-fold significant expression change in *Sin3B$^{p-/-}$ Kras^{pG12D}* compared with *Sin3B$^{p+/-}$ Kras^{pG12D}* pancreas ($P < 0.05$). Bars represent fold enrichment of the pathway in order of significance (*P* values) listed on the right of the bars. Functional categorizations of differentially expressed genes upon knockout of *Sin3B* were analyzed by Gene Ontology Biological Process (GO_BP) with the DAVID. (**B**) Heat map representation of enriched expression for cytokines, NF-κB, and IL-1α pathways in *Sin3B$^{p+/-}$ Kras^{pG12D}* and *Sin3B$^{p-/-}$ Kras^{pG12D}* pancreata and PDEC lines. Heat map represents top enriched genes in *Sin3B$^{p-/-}$ Kras^{pG12D}* compared with *Sin3B$^{p+/-}$ Kras^{pG12D}* pancreata. NES, normalized enrichment score (red, high expression; blue, low expression). (**C**) Quantitative PCR for *Sin3B* and *Il1a* mRNA expression in PDEC cultures obtained from *Sin3B$^{p+/-}$ Kras^{pG12D}* (black bars) and *Sin3B$^{p-/-}$ Kras^{pG12D}* (gray bars) pancreata. *Sin3B$^{p-/-}$ Kras^{pG12D}* mRNA expression levels are relative to the *Sin3B$^{p+/-}$ Kras^{pG12D}* expression levels. (**D**) Quantitative PCR for *Il1a* mRNA expression in acinar 3D cultures obtained from *Sin3B$^{p+/-}$ Kras^{pG12D}* and *Sin3B$^{p-/-}$ Kras^{pG12D}* mice 1 day, 3 days, and 5 days after plating in 3D culture. Black bars represent *Sin3B$^{p+/-}$ Kras^{pG12D}* cells, and gray bars *Sin3B$^{p-/-}$ Kras^{pG12D}* cells. *Sin3B$^{p-/-}$ Kras^{pG12D}* mRNA expression levels are relative to the *Sin3B$^{p+/-}$ Kras^{pG12D}* expression levels. *$P < 0.01$; **$P < 0.05$.

which identify senescent cells in PanINs (11). As expected, we detected p-HP1γ–positive ductal cells in *Sin3B$^{p+/-}$ KRas^{pG12D}* lesions (Figure 3C). In contrast, p-HP1γ was undetectable in any of the rare lesions we could monitor in *Sin3B$^{p-/-}$ KRas^{pG12D}* mice (Figure 3C). We validated these results in 24-week-old *Sin3B$^{p+/-}$ KRas^{pG12D}* and *Sin3B$^{p-/-}$ KRas^{pG12D}* pancreata (Supplemental Figure 3A). To the same extent, DEC1 was not detectable in the *Sin3B$^{p-/-}$ KRas^{pG12D}* lesions at 8 weeks compared with the same grade lesions in *Sin3B$^{p+/-}$ KRas^{pG12D}* pancreata (Figure 3D). To confirm that the drastic reduction in senescent ductal cells observed in *Sin3B$^{p-/-}$ KRas^{pG12D}* pancreata is not merely due to the difference in the stage of the pancreatic lesions, we quantified the percentage of DEC1-positive ductal cells in lesions of each grade (Figure 3E). DEC1 expression was present significantly less in the residual metaplastic lesions and PanIN at 6 to 8 weeks in the *Sin3B$^{p-/-}$ KRas^{pG12D}* compared with *Sin3B$^{p+/-}$ KRas^{pG12D}* pancreata. Similarly, cells composing PanINs in 24-week-old *Sin3B*-deleted mice expressed significantly less DEC1 than those found in their *Sin3B*-expressing counterparts (Figure 3E). Importantly, the selected SIN3B-expressing cells that formed tumors in the *Sin3B$^{p-/-}$ KRas^{pG12D}* mice also expressed DEC1 (Supplemental Figure 3), reinforcing the correlation among SIN3B expression, senescence, and tumor progression.

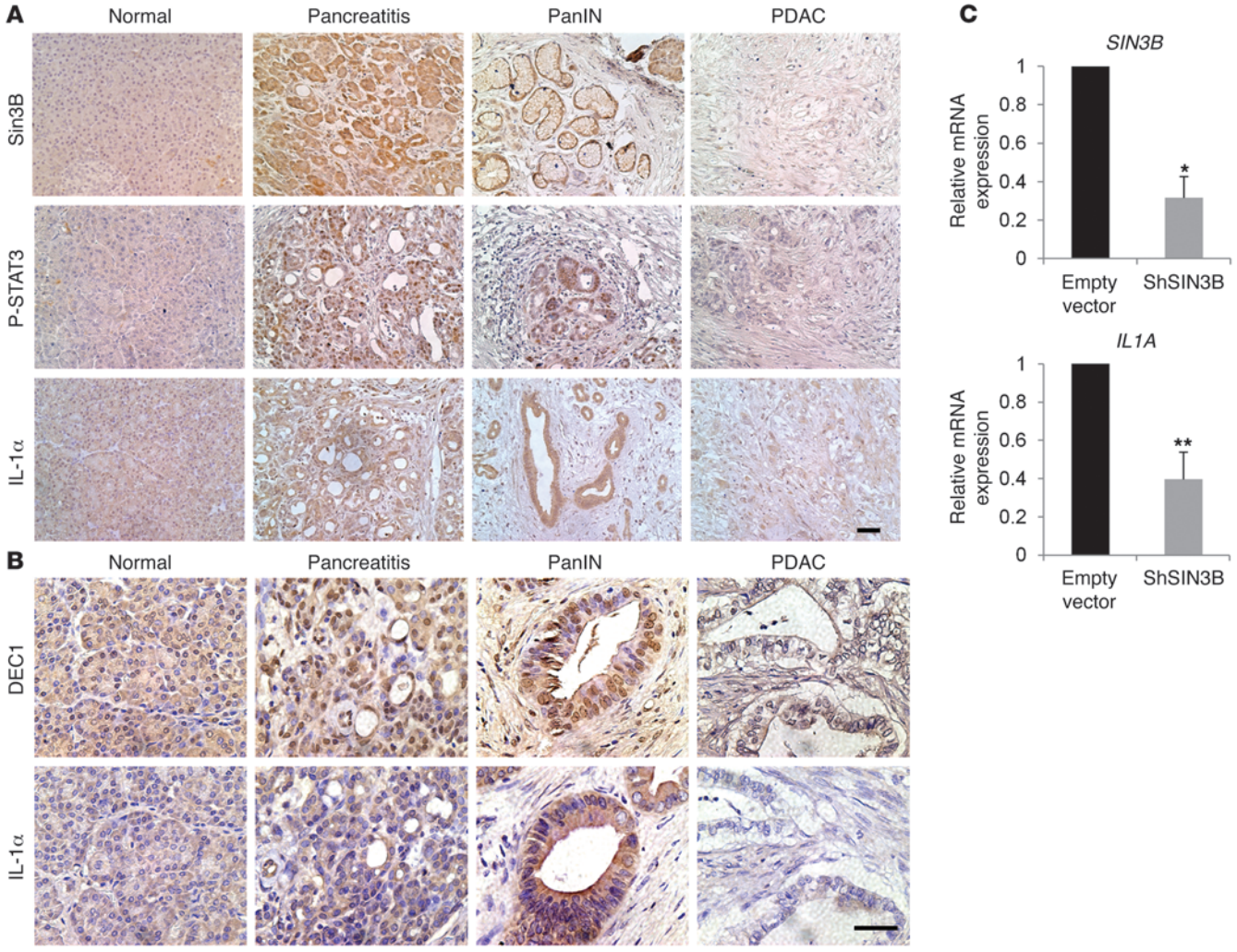

Figure 6

SIN3B levels correlate with an inflammatory response in both human pancreatic tissue and cancer cells. (**A**) Immunohistochemical staining for SIN3B, p-STAT3, and IL-1α in human pancreatic tissue microarrays. Representative IHC staining is shown for normal pancreas, pancreas presenting pancreatitis, PanINs, and PDAC. (**B**) Immunohistochemical staining for DEC1 and IL-1α in human pancreatic tissue microarrays. Representative IHC staining is shown for normal pancreas, pancreas presenting pancreatitis, PanINs, and PDAC. Scale bars: 50 μm. (**C**) Quantitative PCR for *SIN3B* and *IL1A* mRNA expression in AsPc1 pancreatic cancer cells infected with empty vector (black bars) or shRNA against *SIN3B* (shSIN3B, gray bars). **P* < 0.005; ***P* < 0.05. shSIN3B mRNA expression levels are relative to the empty vector expression levels.

Loss of Sin3B mitigates oncogenic KRAS-driven inflammatory response in vivo. Since we observed markedly fewer senescent cells in the *Sin3B*-deleted pancreas and recent reports demonstrated that senescence-associated inflammation can be a protumorigenic event (18, 45), we investigated whether the inflammatory response was affected by *Sin3B* deletion. $Sin3B^{p+/-}$ $KRas^{pG12D}$ pancreata at 6 weeks of age presented extensive Masson trichrome staining, marking desmoplastic tissue (Figure 4A). In contrast, $Sin3B^{p-/-}$ $KRas^{pG12D}$ pancreata only exhibited localized desmoplasia associated with rare PanINs at up to 24 weeks (Figure 4A). Likewise, immune infiltration (CD45-, CD68-, and F4/80-positive cells) was limited and highly localized in *Sin3B*-deficient animals compared with controls (Figure 4, B and D), when analyzed before 24 weeks of age. Inflammation in evolving PanINs is associated with a positive feedback loop of cytokine secretion involving pancreatic cells, immune cells, and cancer-associated fibroblasts (CAF) (25, 26). Neoplastic cells mediate this process by secreting inflammatory cytokines, including IL-1α and IL-6, which are induced upon oncogenic KRAS expression through activation of the ERK1/2, STAT3, and NF-κB pathways (27). Consistently, cells from $Sin3B^{p+/-}$ $KRas^{pG12D}$ PanINs presented strong nuclear signals for activated STAT3 (p-STAT3), ERK1/2 (p-ERK1/2), and p65 (active P65), whereas staining was virtually absent in the corresponding *Sin3B*-deleted cells (Supplemental Figure 4A). Western blots on pancreata whole-cell extracts confirmed the strong decrease in STAT3 and ERK1/2 activation upon *Sin3B* deletion (Supplemental Figure 4B). These effects were associated with a strong decrease in the abundance of *Il6* and *Il1a* transcripts in the *Sin3B*-deleted pancreas compared with their *Sin3B*-expressing littermates at 6 to 8 weeks and at up to 24 weeks for *Il1a* (Figure 4C and Supplemental Figure 4C). Thus, the delayed progression of PanINs caused by *Sin3B* deletion is associated with a pronounced impairment of the inflammatory response.

SIN3B is required for cell-autonomous Il1a expression. We next sought to determine whether SIN3B regulated KRAS-induced *Il1a* and *Il6* expression in a cell-autonomous manner. To this end, gene expression was profiled in *Sin3B*$^{p+/-}$ *KRas*^{pG12D} and *Sin3B*$^{p-/-}$ *KRas*^{pG12D} pancreata and compared with that of cultured primary pancreatic duct epithelial cells (PDEC) of the same genotype. Gene Ontology (GO) and pathway analysis using the Database for Annotation, Visualization and Integrated Discovery (DAVID) functional annotation tool revealed that the immune response was significantly perturbed in the *Sin3B*$^{p-/-}$ *KRas*^{pG12D} pancreata compared with their *SIN3B*-expressing counterparts (Figure 5A and Supplemental Figure 5A). In contrast to whole pancreata, few SIN3B-dependent changes were identified in primary PDEC cultures (Figure 5B and data not shown). For example, *Il6* levels or the NF-κB and the IL-1R pathways were mostly downregulated in *Sin3B*$^{p-/-}$ *KRas*^{pG12D} pancreata compared with *Sin3B*$^{p+/-}$ *KRas*^{pG12D} pancreata, but were not affected by the loss of *Sin3B* in PDEC cell lines (Figure 5B). Strikingly, *Il1a* stood out as one of the rare cytokines affected by *Sin3B* inactivation in both pancreata and PDEC lines (Figure 5B). Further validating these observations, a significant reduction in *Il1a* expression, but not *Il6,* was detected in 2 additional *Sin3B*$^{p-/-}$ *KRas*^{pG12D} PDEC cell lines compared with their *Sin3B*$^{p+/-}$ *KRas*^{pG12D} PDEC counterparts (Figure 5C and Supplemental Figure 5B). We extended these findings in acinar cultures isolated from *Sin3B*$^{p+/-}$ *KRas*^{pG12D} and *Sin3B*$^{p-/-}$ *KRas*^{pG12D} mice, which revealed a specific reduction in *Il1a* transcript levels in the *Sin3B*-deleted primary cells undergoing ADM (Figure 5D and Supplemental Figure 5C). Thus, SIN3B functions in a cell-autonomous manner to promote oncogenic KRAS-driven *Il1a* expression in pancreatic cells.

IL-1α expression correlates with senescence in the pancreas. Our findings thus far indicate that *Sin3B* deletion impairs senescence and *Il1a* induction and leads to a delay in PanIN initiation in the pancreas. IL-1α has recently been shown to serve as an upstream regulator of SASP production (45). We next investigated whether the reduction of *Il1a* expression and the delay in lesion progression observed after *Sin3B* deletion were dependent on the senescence process. To do so, we generated *Sin3B*$^{p+/-}$ *KRas*^{pG12D} *Ink4a/Arf*$^{flox/flox}$ and *Sin3B*$^{p-/-}$ *KRas*^{pG12D} *Ink4a/Arf*$^{flox/flox}$ mice (hereafter referred to as *Sin3B*$^{p+/-}$ *KRas*^{pG12D}*Ink4a*$^{p-/-}$ and *Sin3B*$^{p-/-}$ *KRas*^{pG12D} *Ink4a*$^{p-/-}$), since deletion of the *Ink4a/Arf* locus results in the bypass of senescence (46, 47). As expected *Ink4a*-deleted mice developed PDAC with a low latency, consistent with impaired proliferation control (Supplemental Figure 6, A and B). Both *Sin3B*$^{p+/-}$ *KRas*^{pG12D} *Ink4a*$^{p-/-}$ and *Sin3B*$^{p-/-}$ *KRas*^{pG12D} *Ink4a*$^{p-/-}$ mice exhibited advanced pancreatic cancer and diffuse CK19 expression (Supplemental Figure 6, B and C). Indeed, upon concomitant deletion of the *Ink4a/Arf* locus and KRAS activation, *Sin3B* deletion failed to confer any protection against cancer incidence, suggesting that in a context in which senescence is disabled, SIN3B does not affect cancer progression. Absence of SA–β-gal staining and lack of *p15INK4B* and *Dec1* expression confirmed the bypass of senescence in the *KRas*^{pG12D} *Ink4a*$^{p-/-}$ pancreas, regardless of the *Sin3B* status (Supplemental Figure 6, D and E). Interestingly, despite extensive immune cell infiltration, the bypass of senescence in *KRas*^{pG12D} *Ink4a*$^{p-/-}$ pancreas correlated with the lack of *Il6* and *Il1a* expression (Supplemental Figure 6, F and G). Thus, in mouse pancreata, the expression of *Il1a* is positively correlated with senescence. Moreover, the diminished tumor progression caused by *Sin3B* deletion is paradoxically associated with its ability to promote senescence, suggesting a protumorigenic role for SIN3B-associated senescence in PDAC progression.

SIN3B levels correlate with an inflammatory response in human pancreatic tissue and cancer cells. To investigate the relevance of SIN3B in human PDAC, we examined SIN3B expression using a human tissue array composed of 180 specimens, including normal pancreas, pancreatitis, PanIN lesions, and PDAC. SIN3B was scarcely detected in control human pancreas and PDAC sections, but was strongly upregulated in both pancreatitis and PanINs, consistent with our previous observations in mouse tissues (Figure 6A) (34). Interestingly, in most samples with high levels of SIN3B expression, we also observed p-STAT3 and IL-1α positivity, specifically at the sites of ADM and in PanIN lesions (Figure 6A). We also documented senescence in the pancreas by assessing DEC1 expression, a hallmark of senescence, on serial sections from the same human tissue array (Figure 6B). Consistent with our results in the mouse, several samples exhibited strong positivity for both DEC1 and IL-1α expression, especially in pancreatitis and PanINs lesions (Figure 6B). Based on these observations, we hypothesized that SIN3B may modulate *IL1A* expression in human pancreatic cells. Accordingly, expression of shRNAs targeting *SIN3B* (*shSIN3B*) in AsPc1 and BxPc3 human PDAC cells resulted in a marked reduction in *IL1A* expression levels (Figure 6C and Supplemental Figure 7), suggesting that SIN3B and IL-1α levels are positively and functionally correlated in human pancreatic cells. Together, these results indicate that SIN3B and its associated activities could serve as therapeutic targets to prevent inflammation and pancreatic cancer progression.

Discussion

Senescence has commonly been considered a tumor-suppressive mechanism (48). Our recent discovery that the chromatin modifier SIN3B mediates RAS-induced senescence in mouse fibroblasts coupled with our observation that SIN3B is upregulated in RAS-driven PanINs initially hinted toward a tumor-suppressive role for SIN3B in the pancreas (34). We demonstrate here that genetic inactivation of the chromatin-associated SIN3B protein impairs the occurrence of oncogene-induced senescence in vivo and results in a cell-autonomous defect in KRAS-driven production of the proinflammatory IL-1α cytokine. While we cannot exclude the possibility that inflammation acts independently of senescence to promote pancreatic cancer progression, these results point, for what we believe is the first time, to a protumorigenic effect of senescence in PDAC progression in vivo.

In agreement with our observations, a recent study indicated that the senescence secretome promotes liver cancer progression (21). However, the molecular factors that link oncogene activation to SASP expression remain largely elusive. IL-1α production has been described as the initiating event in the establishment of the SASP in cultured cells (49). In addition, a recent study indicated that disabling the IL-1R/IL-1α pathway partially prevents oncogene-induced senescence and paracrine senescence (50). Finally, recent studies demonstrate a critical function for IL-1α in the initiation of the proinflammatory phenotype in the pancreas (26, 28–30). It is tempting to speculate that upon oncogene activation, SIN3B, through a cell-autonomous upregulation of IL-1α, drives SASP production and promotes a proinflammatory tumor microenvironment. Therefore, our study places the chromatin-associated SIN3B protein at the nexus of senescence and inflammation and further supports a central role for IL-1α in initiating proinflammatory cytokine production in PDAC. It will be of interest to assess whether SIN3B and the associated SASP

mediate the protumorigenic inflammatory microenvironment seen in other cancers and will therefore represent a new strategy for the treatment of diverse inflammatory cancers.

Consistent with the results presented here in pancreatic cells, we also observed a strong reduction in oncogenic RAS-driven *Il1a* expression in *Sin3B*-null mouse embryonic fibroblasts, suggesting that SIN3B-dependent regulation of *Il1a* expression is not tissue specific (G. David, unpublished observation). Given the known repressive activity of SIN3B and its associated complex, these results suggest that the effect of SIN3B on IL-1α production is likely indirect. However, our transcriptomic analysis failed to identify potential intermediate factors that positively regulate *Il1a* levels, while being repressed by SIN3B. An alternative explanation for this positive regulation of IL-1α by SIN3B may stem from our recent observation that SIN3B participates in the release of polymerase pausing at active promoters, thus modulating the levels of actively transcribed genes (51).

Intriguingly, all pancreata with PDAC were positive for SIN3B expression regardless of the *Sin3B* status. Kawaguchi and colleagues previously described the *p48* locus as being transcriptionally silent in approximately 5% of pancreatic ductal cells (36). Coupled with our observation of a strong counterselection of *Sin3B*-deleted pancreatic cells during PDAC progression, it seems likely that residual *Sin3B*-positive cells had an advantage over *Sin3B*-null cells, further supporting the protumorigenic role of SIN3B in our PDAC mouse model.

Nevertheless, in an *Ink4a/Arf*-deleted mouse model, absence of SIN3B did not confer a survival advantage and *Sin3B* deleted pancreata developed PDAC to the same extent as control animals demonstrating the requirement of senescence for SIN3B to promote PDAC progression. Loss of the *Ink4a/Arf* locus occurs in more than 80% of sporadic human PDAC (1). While SIN3B inhibition may not be a viable therapeutic approach for these patients, our results identify SIN3B inhibition as a potential new avenue of treatment for PDAC patients with an intact *Ink4a/Arf* locus. Accordingly, HDAC inhibitors are currently being tested in association with radiotherapy or chemotherapy in phase I and phase II clinical trials in patients with local, advanced, and metastatic disease (52–54). Furthermore, IL-1α is a central cytokine expressed after acute pancreatitis (55) and preliminary data in our laboratory show that IL-1α positively correlates with ADM maintenance in a mouse pancreatitis model (M. Rielland and G. David, unpublished observations). Since repeated episodes of acute pancreatitis can progress to chronic pancreatitis, a well-known risk factor for PDAC (56), mitigating the effects of acute pancreatitis may offer an approach for lowering the frequency of PDAC in the population. In this regard, inhibiting IL-1α production in the pancreas via the use of SIN3B/HDAC1/2 complex inhibitors could serve as a novel targeted approach for preventing inflammation and facilitating regeneration of the pancreas following acute pancreatitis in human patients. Overall, our study solidifies the relationship between chromatin modifiers and cancer progression, while suggesting a protumorigenic function of senescence in vivo.

Methods

Acinar cell isolation and culture. Primary acinar cell cultures were prepared by modifying published protocols (41, 57, 58). Cultures were maintained on Matrigel (BD Biosciences) using RPMI 1640 Medium (Gibco; Invitrogen) supplemented with 10% FBS, penicillin G, streptomycin, 0.1 mg/ml soybean trypsin inhibitor (Sigma-Aldrich), 1 μg/ml dexamethasone (Sigma-Aldrich), 2% Matrigel (BD Biosciences), and 1% glucose (for details, see Supplemental Methods).

Animal models. The LSL-$KRas^{G12D}$ mice were gifts from Tyler Jacks (Massachusetts Institute of Technology, Cambridge, Massachusetts, USA). Dafna Bar-Sagi (NYU Langone Medical Center, New York, New York, USA) provided the *p48*-Cre mice. The $Ink4a^{L/L}$ mice were gifts from Ron DePinho (MD Anderson Cancer Center, Houston, Texas, USA) and Nabeel Bardeesy (Massachusetts General Hospital, Boston, Massachusetts, USA). The LSL-$KRas^{G12D}$, *p48-Cre*, $Ink4a^{L/L}$, m$Sin3B^{+/-}$, and $mSinB^{L/L}$ strains have been described previously (2, 35–37). The strains were mated to obtain mice with the correct genotypes. All animals were maintained in a mixed C57BL/6-FVB background.

Cell culture. BxPc3 and AsPc1 human pancreatic cancer cell lines were provided by Dafna Bar-Sagi (NYU Langone Medical Center). Cells were cultured in RPMI, 10% fetal bovine serum, sodium pyruvate, hepes, penicillin, and streptomycin. The cultures were maintained in 5% CO_2 at 37°C.

Gene expression microarray analysis. Total RNA from $Sin3B^{+/-}$ $KRas^{G12D}$ and $Sin3B^{-/-}$ $KRas^{G12D}$ pancreata (2 pancreata for each genotype) or PDEC (1 for each genotype) was examined on the Affymetrix GeneChip Mouse Genome 430A 2.0 Array. Data were analyzed using Agilent GeneSpring GX11 (Agilent Technologies) to identify gene probes that showed more than a 1.5-fold change with statistical significance ($P < 0.05$, unpaired *t* test). Data were also analyzed using Affymetrix Expression Console and Gene pattern software for the calculation of average expression levels of each chromosome, with each array normalized with the robust multichip array (RMA) algorithm. GO analysis was then performed by uploading the microarray data to DAVID. The complete microarray data set is available from GEO (GSE54197).

Human pancreatic tissue samples. A pilot TMA of 20 patients with pancreatic cancer and 10 control patients was created. From each patient with pancreatic adenocarcinoma, cores of normal pancreas, pancreatitis, low-grade PanIN lesion, high-grade PanIN lesion, tumors from most cellular areas, tumors from most desmoplastic area, and metastatic tumors to the lymph nodes were submitted. As controls, patients with pancreas resection for neuroendocrine tumor, solid pseudo papillary neoplasm, serous cyst adenoma, or metastatic tumors to the pancreas were used. The nature of the lesions was confirmed by a pathologist for each core. Each TMA consisted of 6 to 7 patients and 2 to 3 controls. The core diameter was 2 mm. Sections (5 μm) were cut from formalin-fixed paraffin-embedded samples for the purpose of IHC. For orientation, a core of liver tissue is used.

Histology and IHC. Mouse pancreata were fixed overnight in 10% formalin (Fisher) and processed for paraffin embedding. For histology, deparaffinized sections (5 μm) were stained with Gill's hematoxylin (Richard-Allan Scientific) and eosin Y (Protocol) followed by an alcohol dehydration series and mounting (Permount; Fisher). Trichrome staining was performed at the NYU School of Medicine Histopathology Core Facility. For Alcian blue staining, deparaffinized sections (5 μm) were stained with Alcian blue solution for 30 minutes at room temperature and counterstained with Gill's hematoxylin; this was followed by an alcohol dehydration series and mounting (Permount; Fisher). For IHC, deparaffinized sections (5 μm) were rehydrated and quenched in 1% hydrogen peroxide/methanol for 15 minutes, and antigen retrieval was performed in 10 mM sodium citrate and 0.1% Tween-20 (pH 6.0) for 15 minutes in a microwave oven. Blocking was done in 10% serum, 1% BSA, and 0.1% Tween-20 for 1 hour at room temperature, followed by incubation with the primary antibodies diluted in 1% BSA overnight at 4°C. The following primary antibodies were used: rabbit anti-SIN3B (Santa Cruz A-20; Novus Biologicals)' rabbit anti–α-amylase (Sigma-Aldrich); rat anti-CK19 (TromaIII, developed by Rolf Kemler and obtained from Developmental Studies Hybridoma Bank); rabbit anti–p-STAT3 (Tyr705) (D3A7) (Cell

Signaling), rabbit anti-HP1γ (phospho S83) (Abcam); rat anti-mouse F4/80 (eBioscience); mouse anti-CD68 (KP1) (Abcam); rat anti-mouse CD45 (BD Biosciences); mouse anti–NF-κB, P65 active subunit, clone 12H11 (Millipore); rabbit anti–IL-1α (Abcam); rabbit anti-DEC1 (gift from Adrian Harris, University of Oxford, Oxford, United Kingdom), and rabbit anti–p-p44/42 MAPK (Thr202/Tyr204) (Cell Signaling). After incubating with secondary biotinylated antibodies and solution T.U. horseradish peroxidase streptavidin (both from Vector Laboratories), sections were developed with DAB Peroxidase Substrate Kit (Vector Laboratories). After counterstaining with Gill's hematoxylin (Sigma-Aldrich), slides were subjected to an alcohol dehydration series and mounted with Permount (Fisher). Slides were examined on a Zeiss AxioImager A2 microscope.

Infection of pancreatic cancer cells. DNA sequence encoding an shRNA for *Sin3B* (*shSIN3B*) was chosen to clone into the *pLKO* retroviral vector (Empty Vector; Open Biosystem). BxPc3 and AsPc1 cells were infected with *shSIN3B* or *pLKO* for 3 days and selected in puromycin for 5 days. The level of *Sin3B* knockdown by *shSIN3B* was determined by quantitative RT-PCR.

Immunoblot analysis. Cells were lysed in 1× RIPA buffer (1% NP-40, 0.1% SDS, 50 mM Tris-HCl, pH 7.4, 150 mM NaCl, 0.5% sodium deoxycholate, 1 mM EDTA), 0.5 μM DTT, 25 mM NaF, 1 mM sodium vanadate, 1 mM PMSF, and protease inhibitors. The following primary antibodies were used: rabbit anti–p-p44/42 MAPK (Thr202/Tyr204) (Cell Signaling); mouse anti-ERK (Cell Signaling); rabbit anti–p-STAT3 (Tyr705) (D3A7) (Cell Signaling); and rabbit anti-STAT3 (Cell Signaling). After incubation with either the secondary IRDye Alexa Fluor 680 goat anti-mouse antibody or 800 goat anti-rabbit antibodies (Odyssey), the membranes were visualized with the Odyssey Infrared Imaging System (Li-Cor).

Immunofluorescence. Pancreata were removed, fixed in 4% paraformaldehyde overnight, washed in a 10% sucrose solution, and snap-frozen in OCT compound (Tissue-Tek). Frozen sections of 5 μm were air dried, permeabilized with 0.2% Triton X-100 for 20 minutes, and blocked with 10% serum/0.1% Tween-20 for 1 hour. Slides were incubated with primary antibodies diluted in 1% BSA/0.1% Tween-20 overnight at 4°C. Slides were then incubated with Alexa Fluor–labeled secondary antibodies (Invitrogen), diluted in 1% BSA for 1 hour, and mounted using Vectashield mounting medium with DAPI (Vector Laboratories). Slides were examined on a Zeiss Axiovert 200M microscope. The following antibodies were used: rat anti-CK19 (TromaIII, developed by Rolf Kemler and obtained from Developmental Studies Hybridoma Bank) and rabbit anti–α-amylase (Sigma-Aldrich). Slides were examined on Zeiss AxioImager A2. The 3D immunofluorescence on ADM spheres was performed as previously described (46). The spheres were counterstained with toproisomerase, and the slides were analyzed with a Zeiss LSM510 microscope.

Isolation and culture of PDEC. Isolation and culture of PDEC were performed as described (46, 57). PDEC were isolated from 5-week-old mice and propagated in Matrigel (BD Bioscience).

RT-PCR and quantitative RT-PCR. Extraction of total RNA from Pancreas and PDECs was performed using RNeasy Mini Kit (QIAGEN). For the pancreas, a piece was snap-frozen and ground, and the frozen powder was added to the RNeasy lysis buffer. Reverse transcription was done using Moloney murine leukemia virus polymerase and oligo(dT) primers. RT-PCR analyses were done using Taq DNA polymerase (5 Prime) and dNTP (Promega). Quantitative RT-PCR analyses were done using the SYBR Green method (for primer sequences see Supplemental Methods), and samples were run on the Bio-Rad I Cycler MyiQ. Expression levels were normalized to GAPDH. Results were reported as relative to the abundance of *Sin3B*$^{+/-}$ or *Sin3B*$^{+/-}$ *KRas*^{G12D} transcripts.

SA–β-gal assay. Frozen sections of pancreatic tissue were fixed with 2% formaldehyde/0.2% glutaraldehyde in PBS for 3 to 5 minutes, washed with PBS, and stained at 37°C for 12 to 16 hours in X-Gal solution (1 mg/ml X-Gal, 5 mM potassium ferrocyanide, 5 mM potassium ferricyanide, and 1 mM $MgCl_2$ in PBS at pH 6.0). After counterstaining with eosin (Richard-Allan Scientific), slides were subjected to an alcohol dehydration series and mounted with Permount (Fisher) and counterstained with eosin (Protocols). Slides were examined on Zeiss AxioImager A2.

Statistics. Data were analyzed by Student's *t* test (unpaired, 2-tailed) and results were considered significant at $P < 0.05$. Results are presented as mean ± SEM. Survival curves were plotted by the Kaplan-Meier method and compared by the log-rank test.

Study approval. All human tissues were collected using a protocol approved by the NYU School of Medicine Institutional Review Board and were obtained after informed consent. All animal procedures were approved by the NYU School of Medicine Institutional Animal Care and Use Committee.

Acknowledgments

We thank Yuliya Pylayeva-Gupta, Rengin Soydaner, Laura Taylor, and Dafna Bar-Sagi for technical advice and helpful discussions. We are also grateful to Eva Hernando-Monge, Susanne Tranguch, Julien Maruotti, and Caroline Liot for critical reading of the manuscript. We also value the excellent support provided by Paul Zappile and Yutong Zhang from the NYU Microarray Core and the NYU Langone Medical Center Histology Core. We are also thankful to the NYU Genome Technology Core for their support. We are grateful to all members of the David laboratory for helpful discussions during the preparation of the manuscript. This work was funded by the American Cancer Society (115014-RSG-08-054-01-GMC to G. David), the NIH (5R01CA148639 and 5R21CA155736 to G. David; 5T32CA009161 to D.J. Cantor), the Irma T. Hirschl Charitable Trust (to G. David), and the Samuel Waxman Cancer Research Foundation (to G. David).

Received for publication December 9, 2013, and accepted in revised form January 30, 2014.

Address correspondence to: Gregory David, Department of Biochemistry and Molecular Pharmacology, New York University School of Medicine, MSB417, 500 First Avenue, New York, New York 10016, USA. Phone: 212.263.2926; Fax: 212.263.7133; E-mail: gregory.david@nyumc.org.

1. Hezel AF, Kimmelman AC, Stanger BZ, Bardeesy N, Depinho RA. Genetics and biology of pancreatic ductal adenocarcinoma. *Genes Dev*. 2006; 20(10):1218–1249.
2. Aguirre AJ, et al. Activated Kras and Ink4a/Arf deficiency cooperate to produce metastatic pancreatic ductal adenocarcinoma. *Genes Dev*. 2003; 17(24):3112–3126.
3. Guerra C, Barbacid M. Genetically engineered mouse models of pancreatic adenocarcinoma. *Mol Oncol*. 2013;7(2):232–247.
4. Hingorani SR, et al. Preinvasive and invasive ductal pancreatic cancer and its early detection in the mouse. *Cancer Cell*. 2003;4(6):437–450.
5. Hruban RH, et al. Pancreatic intraepithelial neoplasia: a new nomenclature and classification system for pancreatic duct lesions. *Am J Surg Pathol*. 2001; 25(5):579–586.
6. Klein WM, Hruban RH, Klein-Szanto AJ, Wilentz RE. Direct correlation between proliferative activity and dysplasia in pancreatic intraepithelial neoplasia (PanIN): additional evidence for a recently proposed model of progression. *Mod Pathol*. 2002; 15(4):441–447.
7. Bardeesy N, et al. Both p16(Ink4a) and the p19(Arf)-p53 pathway constrain progression of pancreatic adenocarcinoma in the mouse. *Proc Natl Acad Sci U S A*. 2006;103(15):5947–5952.
8. Morton JP, et al. Mutant p53 drives metastasis and overcomes growth arrest/senescence in pancreatic cancer. *Proc Natl Acad Sci U S A*. 2010;107(1):246–251.
9. Kuilman T, Michaloglou C, Mooi WJ, Peeper DS. The essence of senescence. *Genes Dev*. 2010; 24(22):2463–2479.
10. Collado M, et al. Tumour biology: senescence in premalignant tumours. *Nature*. 2005;

436(7051):642.
11. Caldwell ME, et al. Cellular features of senescence during the evolution of human and murine ductal pancreatic cancer. *Oncogene*. 2012;31(12):1599–1608.
12. Michaloglou C, et al. BRAFE600-associated senescence-like cell cycle arrest of human naevi. *Nature*. 2005;436(7051):720–724.
13. Dimauro T, David G. Ras-induced senescence and its physiological relevance in cancer. *Curr Cancer Drug Targets*. 2010;10(8):869–876.
14. Campisi J. Aging, cellular senescence, and cancer. *Annu Rev Physiol*. 2013;75:685–705.
15. Kuilman T, et al. Oncogene-induced senescence relayed by an interleukin-dependent inflammatory network. *Cell*. 2008;133(6):1019–1031.
16. Acosta JC, et al. Chemokine signaling via the CXCR2 receptor reinforces senescence. *Cell*. 2008; 133(6):1006–1018.
17. Wajapeyee N, Serra RW, Zhu X, Mahalingam M, Green MR. Oncogenic BRAF induces senescence and apoptosis through pathways mediated by the secreted protein IGFBP7. *Cell*. 2008;132(3):363–374.
18. Davalos AR, Coppe JP, Campisi J, Desprez PY. Senescent cells as a source of inflammatory factors for tumor progression. *Cancer Metastasis Rev*. 2010; 29(2):273–283.
19. Kuilman T, Peeper DS. Senescence-messaging secretome: SMS-ing cellular stress. *Nat Rev Cancer*. 2009; 9(2):81–94.
20. Rodier F, et al. Persistent DNA damage signalling triggers senescence-associated inflammatory cytokine secretion. *Nat Cell Biol*. 2009;11(8):973–979.
21. Yoshimoto S, et al. Obesity-induced gut microbial metabolite promotes liver cancer through senescence secretome. *Nature*. 2013;499(7456):97–101.
22. Corcoran RB, et al. STAT3 plays a critical role in KRAS-induced pancreatic tumorigenesis. *Cancer Res*. 2011;71(14):5020–5029.
23. Fukuda A, et al. Stat3 and MMP7 contribute to pancreatic ductal adenocarcinoma initiation and progression. *Cancer Cell*. 2011;19(4):441–455.
24. Lesina M, et al. Stat3/Socs3 activation by IL-6 transsignaling promotes progression of pancreatic intraepithelial neoplasia and development of pancreatic cancer. *Cancer Cell*. 2011;19(4):456–469.
25. Pylayeva-Gupta Y, Lee KE, Hajdu CH, Miller G, Bar-Sagi D. Oncogenic Kras-induced GM-CSF production promotes the development of pancreatic neoplasia. *Cancer Cell*. 2012;21(6):836–847.
26. Tjomsland V, et al. Interleukin 1alpha sustains the expression of inflammatory factors in human pancreatic cancer microenvironment by targeting cancer-associated fibroblasts. *Neoplasia*. 2011; 13(8):664–675.
27. Li N, Grivennikov SI, Karin M. The unholy trinity: inflammation, cytokines, and STAT3 shape the cancer microenvironment. *Cancer Cell*. 2011; 19(4):429–431.
28. Ling J, et al. KrasG12D-induced IKK2/β/NF-κB activation by IL-1α and p62 feedforward loops is required for development of pancreatic ductal adenocarcinoma. *Cancer Cell*. 2012;21(1):105–120.
29. Niu J, Li Z, Peng B, Chiao PJ. Identification of an autoregulatory feedback pathway involving interleukin-1α in induction of constitutive NF-κB activation in pancreatic cancer cells. *J Biol Chem*. 2004; 279(16):16452–16462.
30. Melisi D, et al. Secreted interleukin-1α induces a metastatic phenotype in pancreatic cancer by sustaining a constitutive activation of nuclear factor-κB. *Mol Cancer Res*. 2009;7(5):624–633.
31. Wang H, Clark I, Nicholson PR, Herskowitz I, Stillman DJ. The Saccharomyces cerevisiae SIN3 gene, a negative regulator of HO, contains four paired amphipathic helix motifs. *Mol Cell Biol*. 1990; 10(11):5927–5936.
32. Vidal M, Strich R, Esposito RE, Gaber RF. RPD1 (SIN3/UME4) is required for maximal activation and repression of diverse yeast genes. *Mol Cell Biol*. 1991;11(12):6306–6316.
33. Grandinetti KB, David G. Sin3B: an essential regulator of chromatin modifications at E2F target promoters during cell cycle withdrawal. *Cell Cycle*. 2008;7(11):1550–1554.
34. Grandinetti KB, et al. Sin3B expression is required for cellular senescence and is up-regulated upon oncogenic stress. *Cancer Res*. 2009;69(16):6430–6437.
35. David G, Grandinetti KB, Finnerty PM, Simpson N, Chu GC, Depinho RA. Specific requirement of the chromatin modifier mSin3B in cell cycle exit and cellular differentiation. *Proc Natl Acad Sci U S A*. 2008;105(11):4168–4172.
36. Kawaguchi Y, Cooper B, Gannon M, Ray M, MacDonald RJ, Wright CV. The role of the transcriptional regulator Ptf1a in converting intestinal to pancreatic progenitors. *Nat Genet*. 2002;32(1):128–134.
37. Jackson EL, et al. Analysis of lung tumor initiation and progression using conditional expression of oncogenic K-ras. *Genes Dev*. 2001;15(24):3243–3248.
38. De La OJ, et al. Notch and Kras reprogram pancreatic acinar cells to ductal intraepithelial neoplasia. *Proc Natl Acad Sci U S A*. 2008;105(48):18907–18912.
39. Habbe N, et al. Spontaneous induction of murine pancreatic intraepithelial neoplasia (mPanIN) by acinar cell targeting of oncogenic Kras in adult mice. *Proc Natl Acad Sci U S A*. 2008;105(48):18913–18918.
40. Gidekel Friedlander SY, et al. Context-dependent transformation of adult pancreatic cells by oncogenic K-Ras. *Cancer Cell*. 2009;16(5):379–389.
41. Sawey ET, Johnson JA, Crawford HC. Matrix metalloproteinase 7 controls pancreatic acinar cell transdifferentiation by activating the Notch signaling pathway. *Proc Natl Acad Sci U S A*. 2007; 104(49):19327–19332.
42. Acosta JC, et al. A complex secretory program orchestrated by the inflammasome controls paracrine senescence. *Nat Cell Biol*. 2013;15(8):978–990.
43. Tchkonia T, Zhu Y, van Deursen J, Campisi J, Kirkland JL. Cellular senescence and the senescent secretory phenotype: therapeutic opportunities. *J Clin Invest*. 2013;123(3):966–972.
44. Dimri GP, et al. A biomarker that identifies senescent human cells in culture and in aging skin in vivo. *Proc Natl Acad Sci U S A*. 1995;92(20):9363–9367.
45. Rodier F, Campisi J. Four faces of cellular senescence. *J Cell Biol*. 2011;192(4):547–556.
46. Lee KE, Bar-Sagi D. Oncogenic KRas suppresses inflammation-associated senescence of pancreatic ductal cells. *Cancer Cell*. 2010;18(5):448–458.
47. Guerra C, et al. Pancreatitis-induced inflammation contributes to pancreatic cancer by inhibiting oncogene-induced senescence. *Cancer Cell*. 2011; 19(6):728–739.
48. Campisi J. Cellular senescence as a tumor-suppressor mechanism. *Trends Cell Biol*. 2001;11(11):S27–S31.
49. Orjalo AV, Bhaumik D, Gengler BK, Scott GK, Campisi J. Cell surface-bound IL-1alpha is an upstream regulator of the senescence-associated IL-6/IL-8 cytokine network. *Proc Natl Acad Sci U S A*. 2009;106(40):17031–17036.
50. Acosta JC, et al. A complex secretory program orchestrated by the inflammasome controls paracrine senescence. *Nat Cell Biol*. 2013;15(8):978–990.
51. Jelinic P, Pellegrino J, David G. A novel mammalian complex containing Sin3B mitigates histone acetylation and RNA polymerase II progression within transcribed loci. *Mol Cell Biol*. 2011;31(1):54–62.
52. Lane AA, Chabner BA. Histone deacetylase inhibitors in cancer therapy. *J Clin Oncol*. 2009; 27(32):5459–5468.
53. Tinari N, et al. An epigenetic approach to pancreatic cancer treatment: the prospective role of histone deacetylase inhibitors. *Curr Cancer Drug Targets*. 2012;12(4):439–452.
54. Koutsounas I, Giaginis C, Patsouris E, Theocharis S. Current evidence for histone deacetylase inhibitors in pancreatic cancer. *World J Gastroenterol*. 2013; 19(6):813–828.
55. Yasuda H, et al. Cytokine expression and induction of acinar cell apoptosis after pancreatic duct ligation in mice. *J Interferon Cytokine Res*. 1999; 19(6):637–644.
56. Zheng L, Xue J, Jaffee EM, Habtezion A. Role of immune cells and immune-based therapies in pancreatitis and pancreatic ductal adenocarcinoma. *Gastroenterology*. 2013;144(6):1230–1240.
57. Agbunag C, Lee KE, Buontempo S, Bar-Sagi D. Pancreatic duct epithelial cell isolation and cultivation in two-dimensional and three-dimensional culture systems. *Methods Enzymol*. 2006;407:703–710.
58. Agbunag C, Bar-Sagi D. Oncogenic K-ras drives cell cycle progression and phenotypic conversion of primary pancreatic duct epithelial cells. *Cancer Res*. 2004;64(16):5659–5663.